Mon. Not. R. Astron. Soc. **000**, 000–000 (0000) Printed 12 February 2004 (MN LATEX style file v1.4)

XMM-Newton observations of polars in low accretion states

Gavin Ramsay[1], Mark Cropper[1], Kinwah Wu, K. O. Mason[1], F. A. Córdova[2]
W. Priedhorsky[3]

[1] *Mullard Space Science Laboratory, University College London, Holmbury St. Mary, Dorking, Surrey, RH5 6NT, UK*
[2] *University of California, Riverside, CA 92521, USA*
[3] *Los Alamos National Laboratory, MS D436, Los Alamos, NM 87545, USA*

Received:

ABSTRACT

We have made a series of snap-shot observations of 37 polars using *XMM-Newton*. We found that 16 of these systems were in a low, or much reduced, accretion state. Of those, 6 were not detected in X-rays. This suggests that in any survey of polars, around half will be in a low accretion state. We tested if there was a bias towards certain orbital periods: this is not the case. Of the 10 systems which were detected at low, but significant rates in X-rays, 8 showed significant variability in their X-ray light curves. This implies that non-uniform accretion still takes place during low accretion epochs. The bolometric luminosity of these systems is $\sim 10^{30}$ ergs s^{-1}, two orders of magnitude less than for systems in a high accretion state. The X-ray spectra show no evidence of a distinct soft X-ray component. However, the X-ray and UV data imply that such a low temperature component exists: its temperature is low enough for its flux distribution to move outside the bandpass of the X-ray instruments.

Key words: Stars: individual: – UZ For, CP Tuc, FH UMa, CV Hyi, AR UMa, V834 Cen, UW Pic, V393 Pav, V4738 Sgr, RX J0153–59, MN Hya, ST LMi, RX J1313-32, V1033 Cen, RS Cae, MR Ser – Stars: binaries – Stars: cataclysmic variables – X-rays: stars

1 INTRODUCTION

Polars or AM Her systems are accreting binary systems in which material transfers from a dwarf secondary star onto a magnetic ($B \sim$10–200MG) white dwarf through Roche lobe overflow. They vary in brightness over the binary orbital period, which is synchronised with the spin period of the white dwarf. Unlike non-magnetic accreting binaries they do not have a disk and hence a reservoir of material. Therefore when mass transfer ceases, accretion stops. Many systems have been found to have episodes in which the accretion rate is much reduced, or accretion has ceased completely.

The study of Lamb & Masters (1979) showed that when in a high accretion state ($\dot{m}\gtrsim$1 g s^{-1} cm^{-2}), the density of the accreting gas in the accretion column is sufficiently high to maintain a collisional timescale shorter than the cooling timescale and the flow dynamical timescale. The flow is hydrodynamic, and an accretion shock forms near the surface of the accreting white dwarf. The shock heats the accreting material to temperatures of several tens of keV and thereby emits keV X-rays (see Wu 2000 and references therein). There is also a softer X-ray component, due to heating of the surrounding photosphere of the white dwarf by the hard X-ray irradiation or by bombardment of dense blobs in the accreting material.

In contrast, in polars with low accretion rates ($\dot{m}<$ 0.1 g s^{-1} cm^{-2}) collisions can be so inefficient that not only the electrons and the ions become thermally decoupled but also ion-ion collision cannot maintain the flow in hydrodynamic equilibrium. It was suggested that the kinetic energy of the accreting gas is released via Coulomb collisions of charged particles in the photosphere of the white dwarf (Kuijpers & Pringle 1982; Thomson & Cawthorne 1987; Woelk & Beuermann 1992, 1993). The resulting spectrum would be significantly different to that found in the high accretion state. This has been confirmed in X-ray observations of polars seen in high and low accretion states, see eg the low-state spectra of ST LMi (Ramsay, Cropper & Mason 1995) and AM Her (de Martino et al 1998). In particular, the soft X-ray component seen in high accretion states is absent.

However, even during epochs of low accretion rates, the flow is very unsteady, with flares being seen on short timescales and in various wavelengths. In the optical band, AM Her has exhibited flares in the low state (eg Bonnet-Bidaud et al 2000). Flares are also seen in X-rays: in the polar UZ For an accretion event was observed using *XMM-*

Newton at the phase when the primary accretion region was in view (Still & Mukai 2001, Pandel & Cordova 2002). The X-ray spectrum was consistent with a single temperature plasma of temperature ∼4keV: no distinct soft X-ray component was evident.

We have undertaken a survey of 37 polars using *XMM-Newton* (cf Ramsay & Cropper 2003 for a preliminary overview of this survey). For details of those systems observed in a high accretion state, see Ramsay & Cropper (2004) and references therein. Our survey also gives us an indication of how often polars go into a low/off accretion state. This paper reports on those polars which were in a low state, in particular their number, light curves and their spectra.

2 OBSERVATIONS

XMM-Newton was launched in Dec 1999 by the European Space Agency. It has the largest effective area of any X-ray satellite and also has a 30 cm optical/UV telescope (the Optical Monitor, OM: Mason et al 2001) allowing simultaneous X-ray and optical/UV coverage. The EPIC instruments contain imaging detectors covering the energy range 0.15–10keV with moderate spectra resolution. The OM data were taken in two UV filters (UVW1: 2400–3400 Å, UVW2: 1800–2400 Å) and one optical band (V band). The observation log is shown in Table 1. The data obtained using the RGS instrument (den Herder et al 2001) were of very low signal-to-noise and are therefore not discussed further.

The X-ray data were processed using the *XMM-Newton Science Analysis Software* (SAS) v5.3.3. For the EPIC detectors (Strüder et al 2001, Turner et al 2001), data were extracted using an aperture of $40''$ centered on the source position. Background data were extracted from a source free region. The background data were scaled and subtracted from the source data. The OM data were analysed in a similar way using `omichain` and `omfchain` in SAS v5.4. Data were corrected for background subtraction and coincidence losses (Mason et al 2001). We show in Table 1 the mean V mag determined using the OM for each source at the time of our observation.

For a typical polar in a high accretion state (eg V347 Pav, Ramsay et al 2004), we estimate that the count rate will be a factor of ∼4 greater using *XMM-Newton* compared to *ROSAT*. Every source shown in Table 1 was found to have a X-ray count rate which was significantly lower than when it was observed in the *ROSAT* all-sky survey with the exception of AR UMa and ST LMi which were not detected and MR Ser when it was in a low state. However, we extracted two pointed *ROSAT* observations of AR UMa and found no significant detection in either. Further, it has been found to show a high X-ray state and an optical range of ∼14.5–16.5 (Schmidt et al 1999) while ST LMi was found to be bright in X-rays using *EXOSAT* (Beuermann, Stella & Krautter 1984). MR Ser was also detected using *EXOSAT* (Angelini, Osborne & Stella 1990). Using the highest reported count rate and an appropriate model, the expected count rate for MR Ser in a high accretion state using the *XMM-Newton* EPIC pn detector is 4.2 ct/s. We conclude that all 16 systems in Table 1 were in low or low/intermediate accretion states.

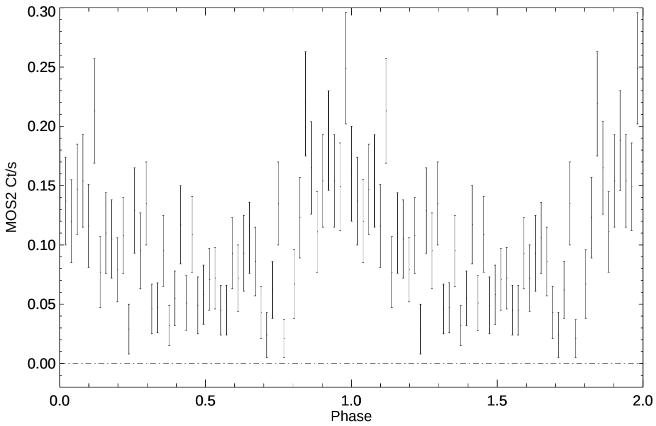

Figure 1. The phased EPIC MOS2 data (0.15–10.0keV) of V834 Cen phased on the ephemeris of Cropper, Menzies & Tapia (1986).

Of these systems, 10 (UZ For, MN Hya, RX J1313–32, CP Tuc, V834 Cen, UW Pic, V393 Pav, ST LMi, V1033 Cen and MR Ser) were detected at low, but significant, levels. We discuss these systems individually in the next section. We do not discuss UZ For since these *XMM-Newton* data have been discussed in detail by Still & Mukai (2001) and Pandel & Cordova (2002).

3 SYSTEMS SHOWING X-RAY VARIATION

3.1 V834 Cen

Sambruna et al (1994) presented multi-epoch observations of V834 Cen using *EXOSAT* and found that the shape of its low energy light curve (0.02–2keV) varied significantly from epoch to epoch. Our EPIC MOS2 X-ray light curve (Figure 1) shows significant flux at all orbital phases and with significant modulation. (Both the EPIC MOS1 and pn data were in timing mode and are therefore not considered further). It is most similar to the 1986 *EXOSAT* light curve (Sambruna et al 1994). However, there is no evidence for an absorption dip at ϕ=0.0, even at lower energies, although this maybe simply due to the relatively poor signal to noise (the accumulated error on the ephemeris of Cropper, Menzies & Tapia 1986 is 0.08 cycles).

We show in Figure 2 the X-ray spectrum taken using the EPIC MOS2 detector. We fitted the spectrum firstly using the stratified accretion column model of Cropper et al (1999). We fixed the mass of the white dwarf at $0.66M_{\odot}$ (Ramsay 2000) and the specific accretion rate at 0.1 g s^{-1} cm^{-2} (appropriate for a system in a low accretion state). We find a fit with χ^2_{ν}=1.49 (42 dof). There is no evidence for a distinct soft X-ray component.

We then fitted the spectrum using a one and two temperature thermal plasma model (the `MEKAL` model in `XSPEC`). A two temperature model gave a much better fit than a one temperature fit. The two temperature model (kT=0.3, 4.3keV) is better than the stratified accretion column model at the 94 percent confidence level. Again there is no evidence for a distinct soft X-ray component. The bolometric luminosity (1×10^{30} ergs s^{-1} d^2_{100}) is typical of systems in a low accretion state (=7.4×10^{29} ergs s^{-1}for d=86 pc, Cropper 1990).

Source	Other Name	Orbit	Date Obs	V	V high state	EPIC pn ct/s	RASS PSPC ct/s	P_{orb} (sec)	EPIC MOS (sec)
UZ For		202	2001-01-14	-	16(1)	0.009(1)	0.70	7590	19394
CP Tuc	AX J2315–592	340	2001-10-17	19.3	17 (2)	0.018(3)	0.24	5364	5395
FH UMa	WGA 1047+6335	342	2001-10-22	20.6	19 (3)	0.025(21)	0.26	4800	7792
CV Hyi	RX J0132–65	362	2001-12-01	20.6	20 (4)	0.002(2)	0.28	4668	7392
AR UMa	1E S1113+432	364	2001-12-03	16.6	14.5 (5)	0.009(8)	0.003	6954	5475
V834 Cen		403	2002-02-19	16.0	14.3 (6)	hw crash	7.8		
		484	2002-07-31	16.5		0.091(4)*		6091	6153
UW Pic	RE J0531–46	415	2002-03-16	18.4	16.4 (7)	0.043(5)	0.73	7980	6192
V393 Pav	RX J1957–57	415	2002-03-16	19.5	18 (8)	0.031(3)	0.9	5929	11687
V4738 Sgr	RX J2022–39	433	2002-04-20	20	18.5 (4)	0.005(2)	0.33	4680	7454
RX J0153–59		438	2002-04-20	19.6	17 (9)	0.005(3)	0.33	4800	7494
MN Hya	RX J0929-24	443	2002-05-10	19.3	17.0 (10)	0.016(3)	0.33	12203	7392
ST LMi		444	2002-05-13	17.7	15 (11)	0.029(3)	0.08	6833	11975
RX J1313-32		484	2002-07-31	16.3	14.6 (12)	0.31(1)	1.9	15084	6884
V1033 Cen	RX J1141–64	489	2002-08-10	20	16.5 (13)	0.044(4)	0.17	11364	11286
RS Cae	RE J0453–42	493	2002-08-19	-	18.4 (14)	-0.013(7)	1.3	5700	9437
MR Ser	PG 1550+191	571	2003-01-22	17.3	15 (15)	0.069(6)	0.04	6814	9030

Table 1. The polars observed in our survey using *XMM-Newton* which were found to be in low accretion state or 'off' accretion state. The 'Orbit' refers to the orbit number of *XMM-Newton* and V was determined using the *XMM-Newton* Optical Monitor. We show the mean count rate derived using the EPIC pn with the exception of V834 Cen which was determined using the EPIC MOS camera. (For sources not clearly detected, we quote the background subtracted count rate for the expected source position). The first observation of V834 Cen was affected by hardware problems. The RASS refers to the *ROSAT* all-sky survey (for AR UMa we used PSPC pointed observations, where it was not significantly detected, and for ST LMi where it was; Ramsay, Cropper & Mason 1995). The duration of the exposure in the EPIC MOS camera is shown in the last column. References for the V high state: (1) Imamura & Steinman-Cameron (1998), (2) Thomas & Reinsch (1996), (3) Singh et al (1995), (4) Burwitz et al (1997), (5) Schmidt et al (1999), (6) Imamura, Steinman-Cameron & Wolff (2000), (7) Reinsch et al (1994), (8) Thomas et al (1996), (9) Beuermann et al (1999), (10) Sekiguchi, Nakada & Bassett 1994 (11) Cropper (1986), (12) Thomas et al (2000), (13) Motch et al (1996), (14) Burwitz et al (1996), (15) Liebert et al (1982).

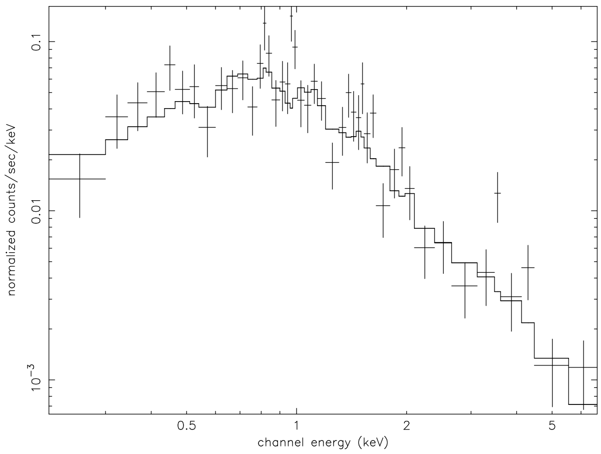

Figure 2. The EPIC MOS2 spectra of V834 Cen. The best fit is shown as a solid line and is an absorbed two temperature thermal plasma model.

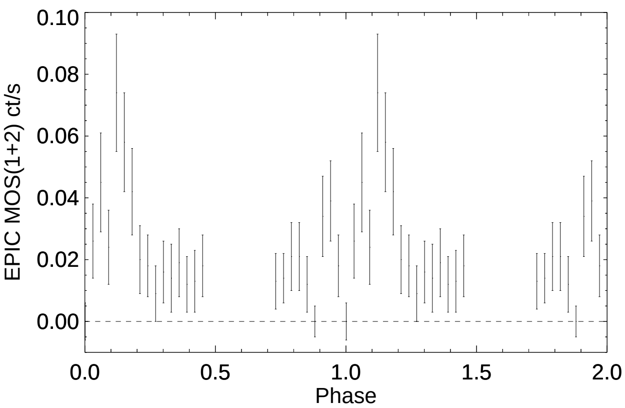

Figure 3. The phased EPIC MOS1+2 data of UW Pic folded on the period of Reinsch et al (1994).

3.2 UW Pic

Reinsch et al (1994) present *ROSAT* survey observations of UW Pic and show that it has 2 maxima per cycle. Unfortunately their ephemeris is not precise enough to allow us to phase our data on their phase convention. However, we do find evidence for a variation in the X-ray light curve which is similar in shape to the *ROSAT* light curve, although the count rate is much lower (Figure 3). The signal to noise of the integrated spectrum is low. However, if we fit an absorbed two temperature plasma model (kT=0.5, 5keV) to the EPIC pn spectrum, we find an absorbed, bolometric luminosity of 1×10^{30} ergs s^{-1}for a distance of 300 pc (Reinsch et al 1994). We find no evidence for a distinct soft X-ray component.

3.3 V393 Pav

Optical and X-ray observations reported by Thomas et al (1996) show V393 Pav to be a one-pole system with a bright phase lasting around 0.5 cycles. Based on the spectroscopic ephemeris the bright phase occurs at ϕ ~0.7-1.2. The accumulated error on the ephemeris up to the date of the *XMM-Newton* observations is 0.10 cycles. We show in Figure 4 the

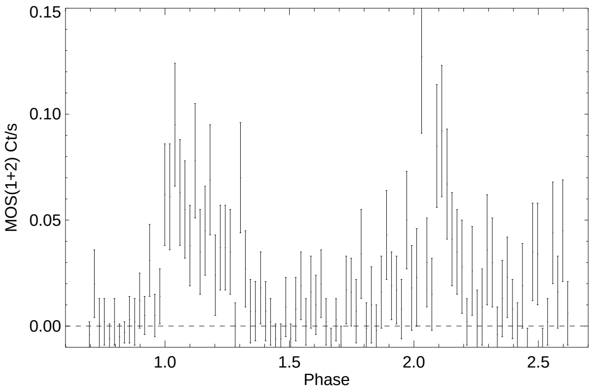

Figure 4. The EPIC MOS (1+2) data of V393 Pav phased on the ephemeris of Thomas et al (1996).

0.15–10.0keV light curve derived using *XMM-Newton* EPIC pn data. These data show a variable light curve with significant flux occurring at $\phi \sim$0.0–0.4, although the bright phase in the second orbital cycle is more narrow than the first. Although the signal to noise of the spectra were low, we fitted them with an absorbed one-temperature thermal plasma model (kT=4.5keV) and obtain a good fit and an unabsorbed bolometric luminosity of 1.3×10^{30} ergs s^{-1}assuming a distance of 350 pc (Thomas et al 1996). There was no evidence for a distinct soft X-ray component.

3.4 ST LMi

ST LMi was not detected during the *ROSAT* all sky survey. Further, when it was the subject of a dedicated observation using *ROSAT* it was detected at the low count rate of 0.1 ct/s (Ramsay, Cropper & Mason 1995). In contrast, the *EXOSAT* observations of ST LMi show the system to be in a high accretion state and a bright X-ray target (*ibid*): it shows a bright phase lasting from $\phi \sim$0.7–1.1 on the ephemeris of Cropper (1986) which is coincident with the optical bright phase.

We show the 0.15–10.0keV light curve made using EPIC pn data in Figure 5. It covers ~1.5 orbital cycles, with the expected maximum occurring near $\phi \sim$0.0. On the first cycle no appreciable increase in flux is seen at this phase. However, during the next cycle there is an increase in flux lasting $\Delta\phi \sim$0.2 cycles and centered on $\phi \sim$0.0. There is no corresponding increase in the UVW2 count rate.

We extracted a spectrum for the accretion event (which lasted ~1200 sec). We find it can be well modelled using an absorbed 2-temperature thermal plasma model (kT=0.8, 5keV) : no distinct soft X-ray component is required (Figure 6). Using a distance of 128pc (Cropper 1990) we obtain an unabsorbed, bolometric luminosity for the accretion event of 1×10^{30} ergs s^{-1}. Extrapolating this best fit model to UV energies gives 4.3×10^{-19} ergs s^{-1} cm^{-2}Å in the UVW2 filter. This is many orders of magnitude less than that observed ($\sim 1\times10^{-15}$ ergs s^{-1} cm^{-2}Å). This suggests that the unheated white dwarf contributes a large fraction to the UV flux.

If we assume that the X-ray event was due to accretion, we can estimate the mass of the accretion event through,

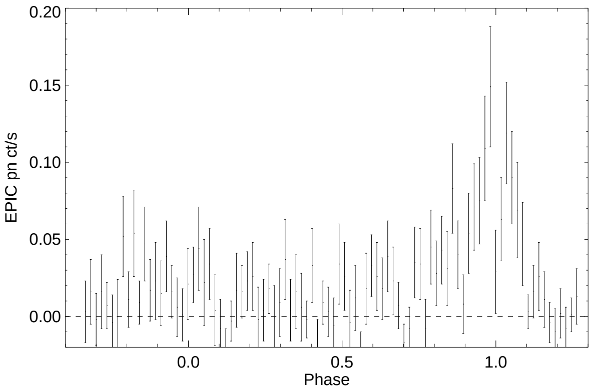

Figure 5. The phased EPIC pn data of ST LMi folded on the ephemeris of Cropper (1986).

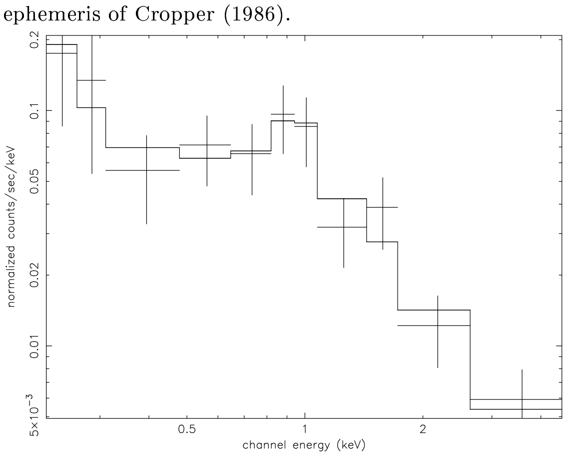

Figure 6. The EPIC pn spectrum of ST LMi fitted using an absorbed blackbody plus 2 temperature thermal plasma model.

$L = GM_1\dot{M}/R_1$, where M_1 and R_1 are the mass and radius of the white dwarf. Assuming M_1=0.7$M_\odot$and $R_1 = 8.6\times10^8$ cm, $\dot{M} = 9.2\times10^{12}$ g s^{-1} or 1.1×10^{16} g for the duration of the event. This is remarkably similar to the mass of the accretion event seen in UZ For (Still & Mukai 2001), although a corresponding increase in the UVW1 band was seen in UZ For. This may imply a different temperature for the reprocessed component in UZ For and ST LMi.

3.5 RX J1313–32

RX J1313–32 was discovered during the *ROSAT* all-sky survey when it was found to be bright reaching a maximum count rate of 6.5 ct/s. When it was observed again using *ROSAT* in two pointed observations, it was found to be much fainter (0.04 ct/s in the PSPC, Thomas et al 2000). Our observations made using *XMM-Newton* show the system reaches a maximum count rate of 0.4 cts/s (EPIC MOS1+2 combined). Using the spectral fit described below we find using `PIMMS` (Mukai 1993) that we would get a count rate in *ROSAT* of 0.01 and 0.03 ct/s in the HRI and PSPC respectively. Although the system shows a low count rate it is still significant and it is likely that RX J1313–32 was observed in an low/intermediate accretion state (Figure 7).

We show the spectrum taken using the EPIC pn detector in Figure 8. There is prominent emission near the Fe Kα line. Closer inspection shows that this is due both to a line

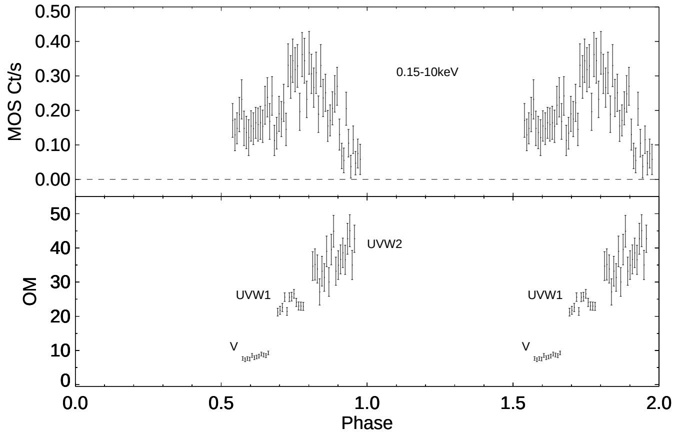

Figure 7. The phased *XMM-Newton* data of RX J1313–32 folded on the ephemeris of Thomas et al (2000). Each bin size is 120s. The units for the OM data are 10^{-16} ergs s^{-1} cm^{-2}Å^{-1}.

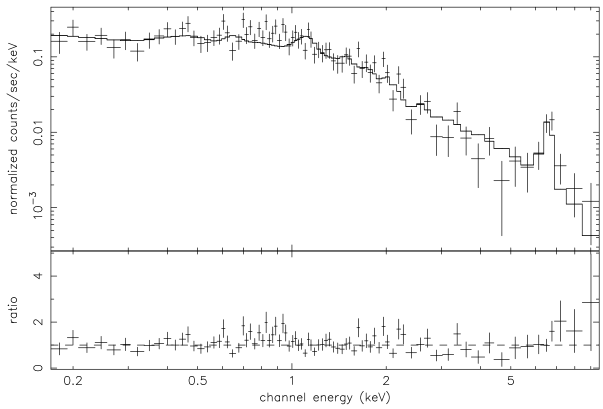

Figure 8. The integrated EPIC pn spectrum of RX J1313-32 together with the best model fit.

at 6.7keV and also the fluorescent line at 6.4keV. The spectrum can be well fit (χ^2_ν=1.04) using a stratified accretion column (Cropper et al 1999). We assumed a white dwarf mass of 0.7$M_\odot$and 0.1 g s^{-1} cm^{-2}. There was no evidence for a distinct soft X-ray component. The unabsorbed bolometric luminosity is 5×10^{30} ergs s^{-1}for a distance of 200pc (Thomas et al 2000).

3.6 V1033 Cen

We show in Figure 9 the 0.15–10.0keV light curve of V1033 Cen folded on the ephemeris of Cieslinski & Steiner (1997). It shows a variation in flux over the orbital period showing maximum near $\phi\sim$ 0.6 and a minimum near ϕ ~0.7–1.2. However, the accumulated error in the phasing is 0.37 cycles. Optical photometry shows a broad maximum around ϕ ~0.0 (Buckley et al 2000). Because of the phase error we cannot be certain whether the X-ray emission originates from this accretion pole.

The spectrum has a low signal-to-noise ratio. However, fitting a one-temperature thermal plasma model (kT=3.5keV) we obtain a luminosity of 1.8×10^{29} ergs s^{-1} d^2_{100} for the integrated spectrum (the distance to V1033 Cen is currently unknown). There is no evidence for a distinct soft X-ray component.

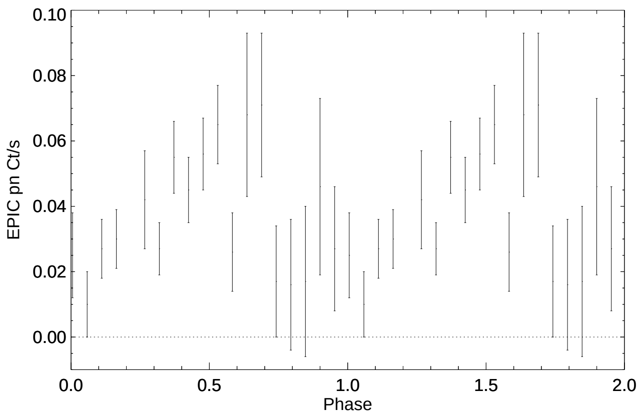

Figure 9. The phased EPIC pn data of V1033 Cen folded on the ephemeris of Cieslinski & Steiner (1997).

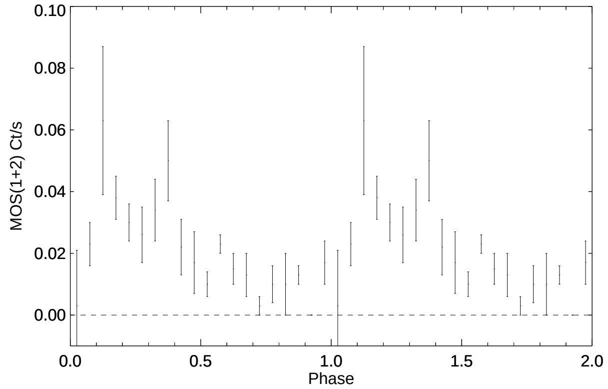

Figure 10. The phased EPIC MOS(1+2) data of MR Ser folded on the ephemeris of Schwope et al (1993).

3.7 MR Ser

MR Ser was discovered using the Palomar Green survey of blue stellar objects (Liebert et al 1982) and classified as a polar based on its optical spectrum and variable polarisation. Our observations of MR Ser show a clear variation in the X-ray flux (Figure 10). It shows a positive signal throughout the orbital cycle with a bright phase lasting ~0.4 cycles. It is reasonably similar to the light curve obtained using *EXOSAT* on April 1 1984 (Angelini et al 1990). MR Ser was also found to be in a low accretion state during both the *ROSAT* all-sky survey and pointed observations. We know of no observations since then which have found MR Ser to be in a high state. We can obtain a good fit to its X-ray spectrum with an absorbed thermal plasma model with temperature ~1.4keV. The unabsorbed bolometric luminosity is $\sim 3\times10^{29}$ ergs s^{-1} d^2_{100}, which for d=139 pc (Schwope et al 1993) gives $\sim 6\times10^{29}$ ergs s^{-1}.

4 SYSTEMS SHOWING NO X-RAY VARIATION

4.1 CP Tuc

Misaki et al (1996) found a new X-ray variable object which they classified as a polar. It showed a strongly modulated light curve which was most prominent at lower energies. Our

Source	M_2 ($M_\odot$)	L_X ($\times 10^{27}$ erg s^{-1})	D (pc)	Observed ($\times 10^{28}$ ergs s^{-1} d^2_{100})	Observed ($\times 10^{28}$ ergs s^{-1})
CP Tuc	0.1	5	>175	3.6(0.6)	11.1 (175pc)
MN Hya	0.3	50	~500	3.2(0.6)	80 (500pc)

Table 2. Those systems which were detected in X-rays but found no X-ray modulation. We show the secondary mass estimated using the mass-period relationship, and the maximum X-ray luminosity assuming the mass-luminosity relationship of Malkov, Piskunov & Shipil'kina (1997) and a saturated X-ray luminosity of $L_X/L_{bol} = 1\times10^{-3}$. We also show the estimated distance and luminosity using the count rate to flux conversion described in the text.

observations show that it was detected at the 6σ level. However, it does not show evidence for a significant modulation.

4.2 MN Hya

MN Hya was discovered during the *ROSAT* all-sky survey. Pointed *ROSAT* observations show a bright X-ray source with an absorption dip just before the eclipse of the secondary star (Buckley et al 1998). The *XMM-Newton* observations show a detection at the 5σ level. There was no significant variation in the light curve.

4.3 The source of X-rays in these systems

Is the source of X-rays in these systems due to accretion at a very low rate or is it due to emission from the secondary star? Late type stars show significant X-ray emission, generally in the form of flaring activity. We now consider if the X-ray flux from these sources can be attributed to the secondary star.

Randich et al (1996) found that in late type systems L_X/L_{bol} does not exceed $\sim 1\times10^{-3}$. We show in Table 2 the secondary mass derived using the standard mass-period relationship and the maximum X-ray luminosity using the mass-luminosity relationship of Malkov, Piskunov & Shipil'kina (1997) assuming a saturated X-ray flux.

A late type secondary would show an X-ray spectrum dominated by a thermal plasma of temperature ~1keV. To estimate the expected count rate, we assume this emission model and set the absorption to be 1×10^{20} cm^{-2}. For the EPIC pn detector and a thin filter, we find that a count rate of 0.01 ct/s would give a luminosity of $\sim 2\times10^{28}$ ergs s^{-1} d^2_{100}.

We find that in both CP Tuc and MN Hya the inferred luminosity is significantly greater than that expected for a late type main sequence star. We conclude that we have not detected the secondary star in either system and the flux is probably due to continuing low-level accretion.

5 THE UV OBSERVATIONS

Out of the 16 systems which were found to be in a low state using *XMM-Newton*, 10 were detected in both the UV filters (UVW1 has an effective wavelength of 2910 Å and UVW2 2120 Å). Another 3 systems (FH UMa, CV Hyi and RS Cae) were detected in the UVW1 filter but not the UVW2 filter. A further 3 systems, (AR UMa, V4738 Sgr and RX J0153–59) were detected in the UV but not in X-rays. UZ For had data taken in only the UVW1 filter while V834 Cen had a technical problem with the UVW2 filter observation. We show in Table 3 the counts in each filter for the 10 systems: we have corrected the observed count rate for coincidence losses (Mason et al 2001).

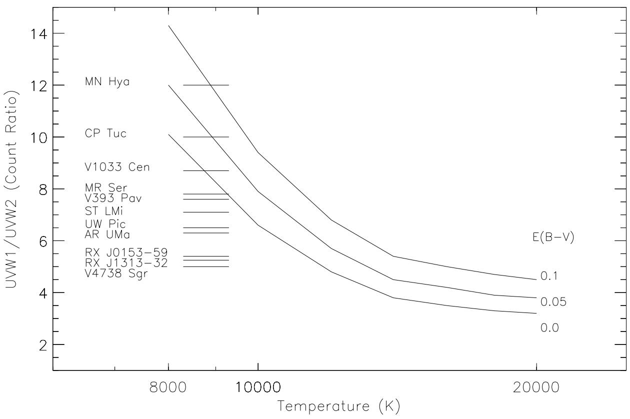

Figure 11. We show the UVW1/UVW2 count rate ratio for different white dwarf temperatures and absorption. We have used Hydrogen white dwarf model atmospheres (those of Koester) and the effective areas of each UV filter. The count ratio for each low state system is marked at the left hand side.

As part of the XMM-OM UV calibration process, 8 white dwarfs of various temperatures have been observed using the OM. These give conversion factors of count rate to flux (1 ct/s in UVW1 corresponds to a flux of 4.4×10^{-16} ergs s^{-1} cm^{-2}Å and 1 ct/s in UVW2 5.8×10^{-15} ergs s^{-1} cm^{-2}Å– taken from the ESA XMM web site). These values give fluxes to within 8 percent of their fluxes at these wavelengths as observed using HST. We show the implied fluxes in the two filters in Table 3.

5.1 Comparing UV count ratios with white dwarf models

We show in Figure 11 the ratio of UVW1/UVW2 counts predicted by convolving white dwarf Hydrogen atmosphere models of different temperatures (those of Detlev Koester) with the effective area curves of the UV filters. We predict the ratios for a range in extinction ($N_H = E_{B-V}4.8\times10^{21}$ cm^{-2}, Bohlin, Savage & Drake 1978). Polars typically have relatively low levels of extinction, so we take an 'upper-limit' of $E_{B-V} = 0.1$. We used the extinction law of Seaton (1979).

The UVW1/UVW2 count ratios shown in Table 3 are all greater than 5. Assuming low extinction this implies temperatures lower than ~14000K. Those systems with the highest ratios (CP Tuc and MN Hya) imply temperatures of ~9000K for low extinction. These temperatures are significantly cooler than the temperatures inferred from UV spectra of polars in a high accretion state: typically an unheated white dwarf has T ~15000-25000K together with a hotter spot (Gänsicke 1998).

5.2 Comparing low state and high state systems

We now compare the UV ratios for systems in the low state with those polars which were observed in a high accretion state (these are taken from Ramsay & Cropper 2004). Table 3 shows that the UVW1/UVW2 Count ratio for the low state systems is >5, with a mean of 7.4. In contrast the high state systems show a ratio <1.2 with a mean of 0.7. There is a clear difference between the high and low state systems: at face value this implies that in the high state the white dwarf is hotter compared with low state.

However, in the high state it is common to have a soft X-ray component which is due to re-processing of hard X-rays from the photosphere of the white dwarf. This will make some contribution to the UV flux. To explore this further, we plot the ratios 0.15–0.5keV/UVW1 (flux) against UVW1/UVW2 (flux) in Figure 12 for the systems shown in Table 3 and also those systems which were observed in a high accretion state. There is a clear separation of low and high state systems, with low state systems lying towards the left hand side, with high state systems in the right hand side.

To determine if these ratios are consistent with that we expect, we estimate the UVW1/UVW2 and 0.15-0.5/UVW1 flux ratios for both low and high state systems. For low state systems we take the best fit X-ray spectral model similar to that of ST LMi (§3.4): namely a two-temperature thermal plasma model. We also add a blackbody component of varying temperature which simulates the unheated white dwarf ($0.7M_{\odot}$and $1.0M_{\odot}$and assume the Nauenberg 1972 mass-radius relationship for white dwarfs) and place it at the distance of ST LMi (128pc Cropper 1990). (Since these estimates are already uncertain and we are using ratios, we use a blackbody rather than a white dwarf model atmosphere for the unheated white dwarf as is sufficient for our purposes). We assume the fraction of the white dwarf which is X-ray heated is much smaller than total surface area. For the high state systems we assume a model consisting of a soft X-ray blackbody component (of varying temperature) and a thermal bremsstrahlung component of temperature 30keV. Further, we assume an X-ray flux distribution consistent with the standard accretion model, ie the soft X-ray luminosity is approximately half that of the hard X-ray luminosity (cf Ramsay & Cropper 2003b). We also include a second blackbody which simulates the unheated white dwarf: we assume a temperature of 20000K (=1.7eV; appropriate for the white dwarf in a high accretion state, Gänsicke 1998) and a $0.7M_{\odot}$white dwarf. We scale the normalisation of this component so that the soft X-ray component due from re-processing covers a fraction of 10^{-4} of the surface of the white dwarf. In both cases we fix the absorption at 5×10^{19} cm^{-2}. For increasing levels of absorption the ratio 0.15–0.5keV/UVW1 will decrease (we include a component for extinction in the UV based on the reddening law of Seaton 1979).

We plot these tracks in Figure 12. For low state systems which have no reprocessed X-ray component we expect their ratio's to lie near the two left hand tracks: eg V1033 Cen, CP Tuc and MN Hya. Systems which have low temperature reprocessed components will lie to the lower right of these tracks: eg MR Ser, UW Pic, RX J1313–32, ST LMi and V393 Pav. Despite the X-ray spectra of the low state systems not requiring a reprocessed X-ray component, our soft X-ray and UV data imply that even in the low state, a reprocessed component exists: it is not detected in X-rays because the temperature is low enough to have moved to energies lower than that of soft X-rays. In this case, the UVW1/UVW2 ratio is insensitive to the temperature of the unheated white dwarf until temperatures of less than ∼5eV are reached.

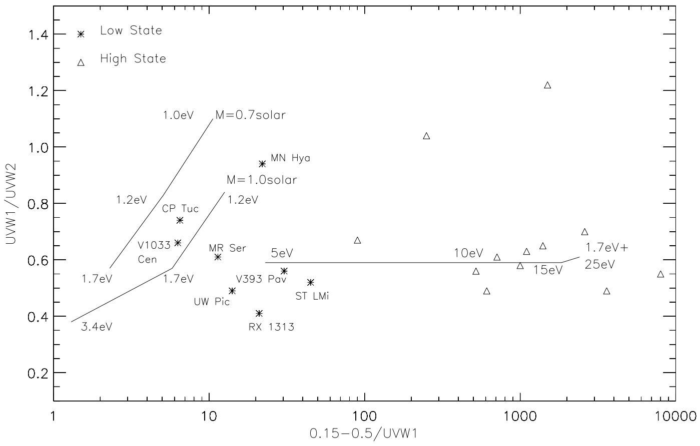

Figure 12. We show the observed 0.15-0.5keV/UVW1 and UVW1/UVW2 flux ratios for those systems in a low accretion state and a high accretion state (taken from Ramsay & Cropper 2004). For high state systems we show the expected ratio assuming a polar with mass $0.7M_{\odot}$ (and using the Nauenberg 1972 relationship) and temperature 1.7eV (=20000K) and which has a spectrum consistent with that predicted by the standard accretion shock model (we show the ratio for various temperatures for the reprocessed soft X-ray component). We also show the expected ratio for low state systems assuming a spectrum like that of ST LMi: we also add a blackbody of various temperature to account for the unheated white dwarf. We assume the interstellar absorption to be 5×10^{19} cm^{-2}.

6 THE FREQUENCY OF SYSTEMS IN A LOW ACCRETION STATE

In our *XMM-Newton* X-ray survey, we observed a sample of 37 systems, which comprises a significant portion of the currently known polars. The orbital periods of this sample range from 77 min to 270 min. Sixteen systems (43 percent) of the systems were found in a state of low or much reduced accretion rate.

Mass transfer in magnetic cataclysmic variables, including polars, is believed to be governed by the orbital evolution of the binary. The frequency of high/low state transitions and the durations of the state duty cycles determine the observed proportion of high or low-state systems. We ask: are the high/low state transition and duty cycle of polars governed by processes dependent on the orbital period? If so, association of the high/low states with the orbital periods will be reflected in our *XMM-Newton* polar survey sample. To verify this we carry out several statistical tests, (i) to examine the bias of the high and low-state systems toward long or short orbital periods, (ii) to verify whether or not there is an alternating sequence of high/low state transition

Source		UVW1		UVW2	0.15–0.5keV	UVW1/UVW2
	Count Rate (Ct/s)	Flux $\times10^{-16}$ ergs s^{-1} cm^{-2}Å	Count Rate (Ct/s)	Flux $\times10^{-16}$ ergs s^{-1} cm^{-2}Å	Flux $\times10^{-15}$ ergs s^{-1} cm^{-2}	(Counts)
CP Tuc	0.60(3)	2.6(1)	0.06(1)	3.5(2)	1.7	10.0
AR UMa	10.08(9)	44.4(5)	1.61(5)	93(2)	-	6.3
UW Pic	1.62(7)	7.1(1)	0.25(2)	14.5(5)	10.0	6.5
V393 Pav	0.53(3)	2.3(1)	0.07(1)	4.1(6)	7.0	7.6
V4738 Sgr	0.15(3)	0.7(1)	0.03(1)	1.7(6)	-	5.0
RX J0153–59	0.42(2)	1.9(1)	0.08(1)	4.7(7)	-	5.3
MN Hya	0.36(3)	1.6(1)	0.03(1)	1.7(2)	3.5	12.0
ST LMi	1.78(3)	7.8(1)	0.25(1)	1.5(6)	35	7.1
RX J1313–32	5.81(8)	26.1(3)	1.10(3)	64(1)	55	5.3
V1033 Cen	0.61(3)	2.7(1)	0.07(1)	4.1(6)	1.7	8.7
MR Ser	3.11(4)	14.0(2)	0.40(2)	23(1)	16	7.8

Table 3. For those systems which were detected in both the UVW1 (peak response 2910 Å) and UVW2 (21210 Å) filters we show their count rate in each filter and the corresponding flux. The number in parenthesis is the error (standard deviation) on the last figure. We also show the observed flux in the 0.15–0.5keV energy band.

(including periodic transition) which can introduce clumping of particle states at certain orbital periods, and (iii) to determine the relative duration of high/low-state duty cycles.

We note that polars have previously been surveyed using *ROSAT*. We therefore also re-analyse the *ROSAT* sample and compare it with our *XMM-Newton* sample. In defining a suitable sample from the *ROSAT* data, we consider all polars which were *not* discovered using the *ROSAT* all-sky survey. We also exclude the very faint systems which may not be detected in the relatively short exposure of the *ROSAT* all-sky survey (eg V1500 Cyg, EU Cnc which are relatively distant systems). We performed a similar study to that done for the *XMM-Newton* sample - namely we compared the count rate for each source determined during the *ROSAT* all-sky survey with other X-ray observations of the same source. Out of a total of 28 systems, 16 (57 percent) were in a low accretion state during the *ROSAT* all-sky observation.

In the statistical analysis of the two samples, we assume that the duration of the high state and low states ($\sim$ weeks, months or longer) are much longer than exposure time of individual systems (typically <10 ksec) during the survey. Under this assumption, the observation of each system can be treated as a snapshot.

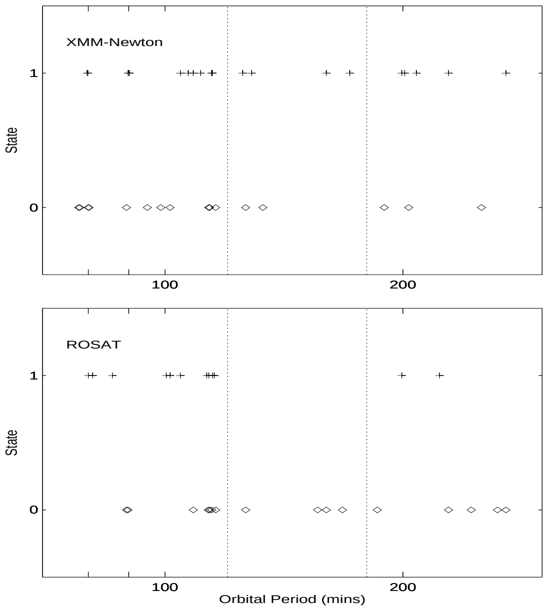

Figure 13. The period distribution of polars in high and low accretion state (assigned with values 1 and 0 respectively) during the *XMM-Newton* survey (top panel) and the *ROSAT* all-sky-survey. We also mark the periods of 120 and 180 min (dotted vertical lines), the approximate boundaries of the period gap, the range of periods where magnetic cataclysmic variables have been claimed to be deficient.

6.1 High/low state duty cycle and orbital-period

As we do not have information about the functional forms of the orbital period distributions of the high-state and the low-state systems, conventional parametric analyses such as those involving the means and the variances of the two distributions are not directly applicable. To overcome this difficulty, we consider non-parametric tests instead. These tests can be applied even for situations in which the numerical scales of the measurements are arbitrary, thus allowing us to examine how the high/low state transition probability is related to the orbital period in an objective manner, without pre-assumed models for the association.

We consider a Wilcoxon-Mann-Whitney rank sum U-test (Wilcoxon 1945, van der Waerden 1969) to search for biases of high and low-state systems towards long/short orbital periods and a general test of randomness (see eg Johnson 1994) to examine the possibility of orbital clumping of high-state and low-state systems. Both tests require the systems to be ranked, and we choose a simple criterion: ranking according to the orbital period. We also adopt the two following conventions in our analysis. (1) The system with the shortest period has the 1st rank, and a higher rank for longer-period systems. (2) Each low-state system is assigned with a state identity parameter of value L, each high-state system with a state identity parameter of value H. The ranks of the systems in the *XMM-Newton* and *ROSAT* surveys are shown in Table 4, while the period distribution of the systems are shown in Figure 13.

XMM-Newton			*ROSAT*		
P_{orb}	H/L?	Source	P_{orb}	H/L?	Source
77.8	L	J0132-65	80.	H	FH UMa
78.0	L	J2022-39	81.02	H	EF Eri
79.7	H	EV UMa	85.8	H	J0425-57
79.9	H	J1015+09	89.4	L	CP Tuc
80.0	L	J0154.0-5947	89.8	L	DP Leo
80.15	L	FH UMa	100.4	H	VV Pup
89.04	L	CP Tuc	101.5	H	V834 Cen
89.8	H	DP Leo	104.6	H	EP Dra
90.08	H	V347 Pav	108.6	L	CE Gru
90.14	H	J1149+28	112.97	H	V2301 Oph
95.0	L	J0453-42	113.47	L	MR Ser
98.8	L	J1957-57	113.64	H	BL Hyi
101.5	L	V834 Cen	113.9	L	ST LMi
104.6	H	EP Dra	114.6	L	WW Hor
107.0	H	J1002-19	114.84	H	AN UMa
108.6	H	CE Gru	115.45	H	EK UMa
110.9	H	J2115-58	115.92	L	AR UMa
113.6	L	MR Ser	126.5	L	UZ For
113.9	L	ST LMi	156.	L	SDSS1324
114.84	H	AN UMa	160.	L	V349 Pav
115.45	H	EK UMa	167.7	L	WX LMi
115.49	H	WW Hor	185.6	L	AM Her
115.92	L	AR UMa	199.3	H	BY Cam
125.4	H	EU Cnc	222.5	H	QQ Vul
126.5	L	UZ For	228.4	L	VY For
128.7	H	J1846+55	244.	L	HS0922+13
133.0	L	J0531-46	263.4	L	SDSS1553
160.0	H	V2009-65	270.	L	V895 Cen
171.3	H	J0501-03			
189.4	L	J1141-6410			
199.3	H	BY Cam			
201.0	H	V1500 Cyg			
203.4	L	MN Hya			
208.0	H	J1007-20			
228.4	H	VY For			
251.4	L	J1313-32			
270.0	H	V895 Cen			

Table 4. The list of sources together with their orbital period and flagged for whether they were in high or low accretion states at the epoch of our *XMM-Newton* survey (left) or the *ROSAT* all-sky survey (right). For reasons of space we have omitted the 'RE' and 'RX' prefix for sources discovered using *ROSAT*.

6.1.1 *Bias in the orbital periods*

First, we verify if there is an excess of either high-state or low-state systems among the long-period polars and among the short-period polars. The null hypothesis is: there is no bias of high-state and low-state systems towards long orbital periods or short orbital periods.

In the *XMM-Newton* sample, the number of low-state systems is $n_1 = 16$ and the number of high-state systems is $n_2 = 21$. The corresponding rank sums of the two types of systems are $W_1 = 268$ and $W_2 = 435$. In the Wilcoxon-Mann-Whitney test, the U-statistic is given by

$$U_i \quad = \quad W_i - \frac{n_i\,(n_i+1)}{2} \qquad (i=1,2)$$

As the numbers of two types of systems are sufficiently large ($n_1 > 10$ and $n_2 > 10$), the U-statistics are described approximately by a normal distribution, with the mean and variance given by

$$\begin{aligned} \mu(U_1) \quad &= \mu(U_2) \quad = \frac{n_1 n_2}{2} \ , \\ \sigma^2(U_1) \quad &= \sigma^2(U_2) \quad = \frac{n_1 n_2 (n_1+n_2+1)}{12} \end{aligned}$$

The associated standardised random variable is defined as

$$z \quad = \quad \frac{U_1 - \mu(U_1)}{\sigma(U_1)} \ .$$

Thus, the statistics that characterise the *XMM-Newton* sample are $U_1 = 132$, $U_2 = 204$ (cf Table 4), $\mu(U_i) = 168$ and $\sigma^2(U_i) = 1064$, implying a standardised random variable $z_{\rm xmm} = -1.10$.

In the *ROSAT* sample, we have $n_1 = 16$ and $n_2 = 11$, so the U statistic can again be approximated by a normal distribution. The rank sums of the two types of systems are $W_1 = 279$ and $W_2 = 127$; the relevant statistics are $U_1 = 143$, $U_2 = 49$, $\mu(U_i) = 96$ and $\sigma^2(U_i) = 464$. The corresponding standardised random variable is $z_{\rm rosat} = +2.18$.

For 99 and 95 percent confidence interval, $-2.575 < z < 2.575$ and $-1.96 < z < 1.96$ respectively. The z value for the *XMM-Newton* sample is well within the 95 percent confidence interval, while the *ROSAT* sample is within the 99 percent confidence interval. Therefore, we cannot reject the null hypothesis on a high significance level to favour the alternative hypothesis.

We note that similar results can be obtained by the Kolmogorov-Smirnov test, which may be inefficient to discriminate the difference in the period distribution of the high-state and low-state systems especially when the difference occurs near the two ends of the period range. The D-statistic that we obtain for the *XMM-Newton* sample is 0.277, corresponding to a probability of 0.49 for the null hypothesis. The *ROSAT* sample has a larger D-statistics, 0.479, and a null-hypothesis probability of 0.09.

As a summary, we conclude that the *XMM-Newton* sample and the *ROSAT* sample do not show significant difference in the (global) distributions of orbital periods among the high-state and low-state systems between 77 and 270 min. That is, there is no firm bias of high-state or low-state systems toward short orbital periods and towards long orbital periods.

6.1.2 *Period clumping of high and low-state systems*

We now test whether the systems in the two accretion states are in a random order when ranked according to their orbital periods. This test will reveal the sequence of alternating high/low states in the population if the alternation depends strongly and explicitly on the orbital period, but it does not exclude such transitional behaviour for each individual system.

The null hypothesis is: the period ordering of the high-state and low-state systems are random. Using our adopted convention, we construct a sequence for the *XMM-Newton* sample: LLHHL... (cf Table 4). We then define a u-statistic, which is the number of runs (see Johnson 1994) in the sequence, and for the *XMM-Newton* sample it is 20. For samples with $n_1 > 10$ and $n_2 > 10$, the u-statistics approximately have a normal distribution. The mean and variance of the distribution given by

$$\mu(u) = \frac{2n_1n_2}{n_1+n_2}+1 \,,$$
$$\sigma^2(u) = \frac{2n_1n_2(2n_1n_2-n_1-n_2)}{(n_1+n_2)^2(n_1+n_2-1)} \,,$$

the standardised random variable of the u-statistic is

$$z = \frac{u-\mu(u)}{\sigma(u)} \,.$$

The statistics of the *XMM-Newton* sample are therefore $u = 20$, $\mu(u) = 19.16$ and $\sigma^2(u) = 8.66$. It follows that the standardised random variable $z_{\rm xmm} = 0.29$.

Similarly, we can order the *ROSAT* systems in a similar manner. This gives $u = 12$, $\mu(u) = 13.71$, $\sigma^2(u) = 6.46$ and $z_{\rm rosat} = -0.67$. As $z_{\rm xmm}$ and $z_{\rm rosat}$ is well within the interval $-1.00 < z < 1.00$, the null hypothesis is consistent with the data of both survey, implying that the period ordering of the systems are probably random. We note that visual inspection may suggest a deficiency of high-state systems with periods between 120 and 180 min (the controversial period gap of polars) in the *ROSAT* sample (Figure 13). However, this apparent deficiency of high-state systems is not seen in the *XMM-Newton* sample. The randomness test that we have performed indicates that any clumpiness in the two sequences can be explained by statistical fluctuation. Combining the result of this test and that in §6.1.1, we conclude that the *XMM-Newton* and *ROSAT* data do not show evidence that the high-state and low-state transition and duty cycle of polars are associated with certain preferred orbital periods.

6.2 Probability of being in the low state

Inspection of the proportion of low-state sources suggests that the fractional duty cycle of low accretion state is 0.5. However, what is the uncertainty in this fraction? We show in the Appendix how we calculate this uncertainty in a formal Bayesian approach.

In the *XMM-Newton* sample $N = 37$ and $k = 16$, and in the *ROSAT* sample $N = 28$ and $k = 16$, where N is the number of systems in the sample and k is the number of systems in a low accretion state. Figure 14 shows the cumulative probability distribution for low-state duty cycle x, which is $P([x,1]|k,N)$, and its derivative for the two surveys. The estimate $\hat{x}$ is 0.442 and the 90% confidence interval is $(0.258, 0.734)$ for the *XMM-Newton* sample. The estimate $\hat{x}$ is 0.585 and the 90% confidence interval is $(0.342, 0.863)$ for the *ROSAT* sample, consistent with the result obtained from the *XMM-Newton* sample. Thus, we may conclude that the probability of a system in a low state is ~50 percent, with an uncertainty corresponding to the two samples given above.

6.3 Implications for the space density of polars

Three new polars were discovered using *EXOSAT* in a coverage of 5 percent of the sky. Based on this finding Hameury, King & Lasota (1990) predicted that around 60 new polars would be discovered using *ROSAT*. Since *ROSAT* was more sensitive than *EXOSAT*), this number would be expected to be greater. In contrast, ~30 polars were discovered using *ROSAT*. However, the Poisson uncertainty of the prediction is ±35. Taking into account of statistical fluctuations, we conclude that the detection of approximately 30 systems by *ROSAT* is consistent with the results of the *EXOSAT* survey.

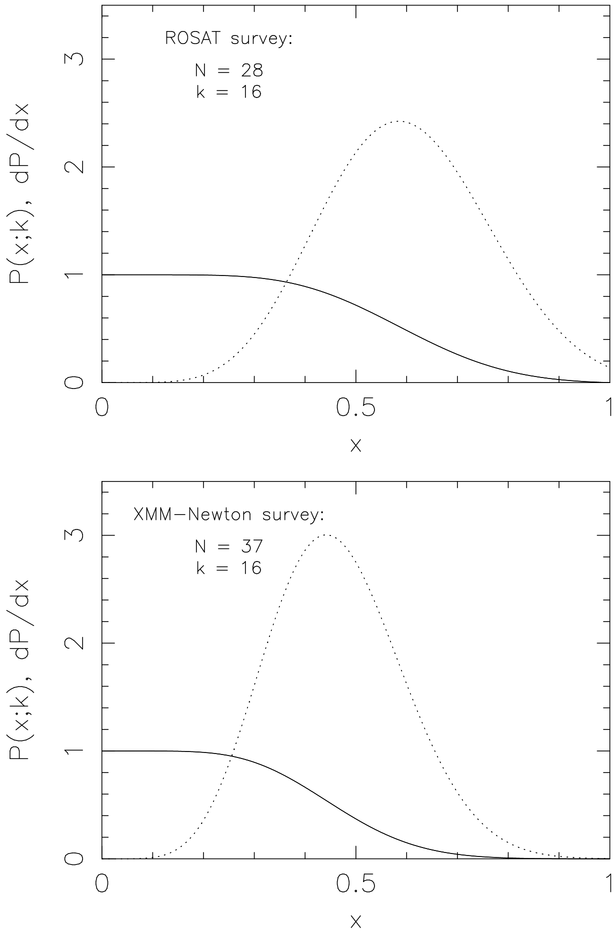

Figure 14. The cumulative probability distribution $P(x;k) \equiv P([x,1] \mid k,N)$ (solid line) for the low-state duty cycle x and its derivative dP/dx (dotted line) for the *ROSAT* and *XMM-Newton* surveys (top and bottom panels respectively). The best estimate of the low-state duty cycle, $\hat{x}$, is given by the peak of dP/dx, and the bounds of the 90% confidence interval are located by $P(x;k) = 0.95$ and 0.05 respectively.

The estimated space density of CVs is $\sim (1-3) \times 10^{-5}$ pc^{-3} (Patterson 1998, Schwope et al 2002a). The polar to disk CV ratio, inferred from the *Einstein* galactic plane survey, is about 1/3 (Hertz et al 1990). Thus, the space density of polars is probably slightly less than 10^{-5} pc^{-3}.

Because of inhomogeneities in the local interstellar medium, soft X-rays sources have very different discovery probabilities in different parts of the sky. Soft X-ray sources such as polars and single white dwarfs, could be preferentially found in certain parts of the sky (eg Warwick et al 1993). Thus, the survey carried out by the *EXOSAT* LE inevitably suffered from this bias.

In addition to the bias due to absorption by an inhomogeneous local interstellar medium, there are several other limiting factors that could also introduce uncertainties in the estimates of the space density of galactic polars. Among them is the lack of accurate distance estimates for many systems (many polars have only lower limits), and the fact that those polars which accrete at an extremely low rate (cf Schwope et al 2002b) are unlikely to be discovered in X-ray surveys. Another important limiting factor is the uncertainties in the proportion of high-state and low-state systems in the population. In deriving the space density for polars, many workers (eg, Thomas & Beuermann 1998) first assumed that the sample is complete at high galactic latitudes, then corrected for parts of the sky (such as the North-Polar Spur) which have higher interstellar absorption and finally rescaled according to the fraction of systems in the high-accretion states. This survey has eliminated one uncertainty by showing that about a half of the polar population is in a low accretion state at a given time.

7 CONCLUSIONS

In our survey of 37 polars using *XMM-Newton* we found that 16 were a low accretion state. Of these, 6 were not detected in X-rays. The *XMM-Newton* data show no evidence that the low state systems are biased towards certain orbital periods. The period ordering of the system is consistent with random. Similar results were found when re-examining a sample of the *ROSAT* all-sky survey data, in which 16 out of 28 systems were in low accretion states.

Of those low state systems which were detected at a significant level, 8 showed a significant variation in X-rays. We find that in epochs with low accretion states, accretion is still occurring, often sporadically at the same accretion pole as when the system is in a high accretion state. Their spectra can be modelled using a two-temperature thermal plasma model of temperature several keV. The unabsorbed bolometric luminosity is typically $\sim 10^{30}$ ergs s^{-1}: this is two orders of magnitude less than the luminosity observed in the high accretion state (Ramsay & Cropper 2003b). There is no evidence for a distinct soft X-ray luminosity as often seen in the high accretion state. However, the UV data suggests that a reprocessed component is still present in the low accretion state, but is cooler than in the high state and therefore shifted into the UV or far-UV.

8 ACKNOWLEDGMENTS

This is work based on observations obtained with XMM-Newton, an ESA science mission with instruments and contributions directly funded by ESA Member States and the USA (NASA). These observations were part of the OM guaranteed time programme. We thank Detlev Koester for kindly supplying white dwarf model atmosphere spectra.

REFERENCES

Angelini, L., Osborne, J. P., Stella, L., 1990, 245, 652
Beuermann, K., Stella, L., Krautter, J., 1984, in Proc Symp X-ray Astronomy, 84, Bologna, ed Tanaka, Y., ISAS, Japan
Beuermann, K., Thomas, H.-C., Reinsch, K., Schwope, A. D., Trmper, J., Voges, W., 1999, A&A, 347, 47
Bohlin, R. C., Savage, B. D., Drake, J. F., 1978, ApJ, 224, 132
Bonnet-Bidaud, J. M., Mouchet, M., Shakhovskoy, N. M., Somova, T. A., Somov, N. N., Andronov, I. L., de Martino, D., Kolesnikov, S. V., Kraicheva, Z., 2000, A&A, 354, 1003
Buckley, D. A. H., Barrett, P. E., Haberl, F., Sekiguchi, K., 1998, MNRAS, 299, 998
Buckley, D. A. H., Cropper, M., van der Heyden K., Potter, S. B., Wickramasinghe, D. T., 2000, MNRAS, 318, 187
Burwitz, V., Reinsch, K., Schwope, A. D., Beuermann, K., Thomas, H.-C., Greiner, J., 1996, A&A, 305, 507
Burwitz, V., Reinsch, K., Beuermann, K., Thomas, H.-C., 1997, A&A, 327, 183
Cieslinski, D., Steiner, J. E., 1997, MNRAS, 291, 321
Cropper, M., 1986, MNRAS, 222, 225
Cropper, M., 1990, Space Sci Rev, 54, 195
Cropper, M., Menzies, J. W., Tapia, S., 1986, MNRAS, 218, 201
Cropper, M., Wu, K., Ramsay, G., Kocabiyik, A., 1999, MNRAS, 306, 684
de Martino, D. et al, 1998, A&A, 333, L31
den Herder, J. W., et al, 2001, A&A, 365, L7
Gänsicke, B., 1998, In Proc 13th N. American workshop on CVs, ASP Conf Series, 137, 88
Hameury, J. M., King, A. R., Lasota, J. P. 1990, MNRAS, 242, 141
Hertz, P., Bailyn, C. D., Grindlay, J. E., Garcia, M. R., Cohn, H., Lugger, P. M., 1990, ApJ, 364, 251
Imamura, J. N., Steiman-Cameron, T. Y., 1998, ApJ, 501, 830
Imamura, J. N., Steiman-Cameron, T. Y., Wolff, M. T., 2000, 112, 18
Johnson, R. A. 1994, Miller and Freund's Probability and Statistics for Engineers, Prentice Hall, Englewood Cliffs
King, A. R., Lasota, J. P., 1979, MNRAS, 188, 653
Kuijpers, J., Pringle, J. E., 1982, A&A, 114, L4
Lamb, D. Q., Masters, A. R., 1979, ApJ, 234, 117
Liebert, J., Stockman, H. S., Williams, R. E., Tapia, S., Green, R. F., Rautenkranz, D., Ferguson, D. H., Szkody, P., 1982, ApJ, 256, 594
Malkov, O. Y., Pishunov, A. E., Shpil'kina, D. A., 1997, A&A, 320, 79
Mason, K. O., et al 2001, A&A, 365, L36
Misaki, K., et al, 1995, IAUC, 6260
Motch, C., Haberl, F., Guillout, P., Pakull, M., Reinsch, K., Krautter, J., 1996, A&A, 307, 459
Mukai, K., 1993, Legacy, 3, 21
Nauenberg M., 1972, ApJ, 175, 417
Pandel, D., Cordova, F. A., 2002, MNRAS, 336, 1049
Patterson J., 1998 PASP, 110, 1132
Ramsay, G., Cropper, M., Mason, K. O., 1995, MNRAS, 276, 1382
Ramsay, G., 2000, MNRAS, 314, 403
Ramsay, G., Cropper, M., 2003, In Proc Cape Town Workshop on mCVs, astro-ph/0301609
Ramsay, G., Cropper, M., Mason, K., Cordova, F., Priedhorsky, W., 2004, MNRAS, 347, 95
Ramsay, G., Cropper, M., 2004, MNRAS, 347, 497
Randich, S., Schmitt, J. H. M. M., Prosser, C. F., Stauffer, J. R., 1996, A&A, 305, 785
Reinsch, K., Burwitz, V., Beuermann, K., Schwope, A. D., Thomas, H.-C., 1994, A&A, 291, L27
Sambruna, R., M., Parmar, A. N., Chiappetti, L., Maraschi, L., Treves, A., 1994, ApJ, 424, 947
Schmidt, G. D., Hoard, D. W., Szkody, P., Melia, F., Honeycutt, R. K., Wagner, R. M., 1999, ApJ, 525, 407
Schwope, A. D., Beuermann, K., Jordan, S., Thomas, H.-C., 1993, A&A, 278, 487
Schwope, A. D., Brunner, H., Buckley, D., Greiner, J., v.d. Heyden, K., Neizvestny, S., Potter, S., Schwarz, R., 2002a, A&A, 396, 895
Schwope, A. D., Brunner, H., Hambaryan, V., Schwarz, R.,

Staude, A., Szokoly, G., 2002b, p102, In ASP Conference Proceedings, Vol. 261. Editors Gänsicke, B., Beuermann, K., Reinsch, K.
Seaton, M. J., 1979, MNRAS, 187, 73P
Sekiguchi, K., Nakada, Y., & Bassett, B., 1994, MNRAS, 266, L51
Singh, K. P., et al, 1995, ApJ, 453, L95
Still, M., Mukai, K., 2001, ApJ, 562, L71
Strüder, L., et al, 2001, 365, L18
Thomas, H.-C., Beuermann, K., Schwope, A. D., Burwitz, V., 1996, A&A, 313, 833
Thomas, H.-C., Beuermann, K., 1998, In Lecture Notes in Physics, Vol 506, *The local bubble and beyond*, Proc IAU Coll 166, p247
Thomas, H.-C., Reinsch, K., 1996, A&A, 315, L1
Thomas, H.-C., Beuermann, K., Burwitz, V., Reinsch, K., Schwope, A. D., 2000, A&A, 353, 646
Thomson, A. M., Cawthorne, T. V., 1987, MNRAS, 224, 425
Turner, M., et al 2001, A&A, 365, L27
van der Waerden, B. L. 1969, Mathematical Statistics, Springer-Verlag, New York
Warwick, R. S., Barber, C. R., Hodgkin, S. T., Pye, J. P., 1993, MNRAS, 262, 289
Wilcoxon, F. 1945, Biometrics, 1, 80
Woelk, U.; Beuermann, K., 1992, A&A, 256, 498
Woelk, U.; Beuermann, K., 1993, A&A, 280, 169
Wu K., 2000, Space Science Reviews, 93, 611

APPENDIX: Determining the probability of being in the low state

The probability of m systems in a low state in a sample of N system is given by a binomial distribution

$$b(m,N;x) \quad = \quad \frac{N!}{m!(N-m)!}\, x^m (1-x)^{N-m} \ ,$$

where x is the low-state duty cycle of the systems. If the systems are not observed simultaneous, it introduces counting fluctuations, which could be approximated by a Poisson process. The probability of k systems in a sample of N systems are observed in the low state during a survey is therefore

$$\begin{aligned} P(k,N \mid x) &= \sum_{m=1}^{N} \frac{e^{-m} m^k}{k!}\, b(m,N;x) \\ &= \sum_{m=1}^{N} \frac{e^{-m} m^k}{k!} \frac{N!}{m!(N-m)!}\, x^m (1-x)^{N-m} \ . \end{aligned}$$

From the Bayesian Theorem, the probability of a system being in a low state given that k systems are observed in a low state is

$$P(a \le x \le b \mid k,N) \quad = \quad \frac{\int_a^b dx\ P(k,N \mid x) f(x)}{\int_1^0 dx\ P(k,N \mid x) f(x)} \ ,$$

where $f(x)$ is a priori probability density distribution of x. For a uniform density distribution $f(x)$, we have

$$P(a \le x \le b \mid k,N) \quad = \quad \frac{I(a,b;k,N)}{I(0,1;k,N)} \ ,$$

and x can be interpreted as the low-state duty cycle. The numerator $I(a,b;k,N)$ is given by

$$\begin{aligned} I(a,b;k,N) &= \sum_{m=1}^{N} \frac{e^{-m} m^k}{k!} \frac{N!}{m!(N-m)!} \\ &\qquad \times \int_a^b dx\ x^m (1-x)^{N-m} \\ &= \sum_{m=1}^{N} \frac{e^{-m} m^k}{k!} \frac{N!}{m!(N-m)!} \\ &\qquad \times \Big[B_b(m+1, N-m+1) - B_a(m+1, N-m+1) \Big] \ , \end{aligned}$$

where $B_b(m+1, N-m+1)$ and $B_a(m+1, N-m+1)$ are incomplete Beta functions. The denominator $I(0,1;k,N)$ is given by

$$\begin{aligned} I(0,1;k,N) &= \sum_{m=1}^{N} \frac{e^{-m} m^k}{k!} \frac{N!}{m!(N-m)!} \\ &\qquad \times \int_0^1 dx\ x^m (1-x)^{N-m} \\ &= \sum_{m=1}^{N} \frac{e^{-m} m^k}{k!} \frac{N!}{m!(N-m)!}\ \frac{\Gamma(m+1)\Gamma(N-m+1)}{\Gamma(N+2)} \\ &= \frac{1}{(N+1)} \sum_{m=1}^{N} \frac{e^{-m} m^k}{k!} \ , \end{aligned}$$

where $\Gamma(m+1)$, $\Gamma(N-m+1)$ and $\Gamma(N+2)$ are Gamma functions.